CORRECTIONS TO THE CONSTITUTIVE EQUATIONS OF PIEZOELECTRIC LAMINATED BEAMS THROUGH A MIXED VARIATIONAL APPROACH

Corrado Maurini, Joël Pouget, Francesco Dell'Isola

CORRECTIONS TO THE CONSTITUTIVE EQUATIONS OF PIEZOELECTRIC LAMINATED BEAMS THROUGH A MIXED VARIATIONAL APPROACH

Corrado Maurini*, Joël Pouget* and Francesco dell'Isola†

* Laboratoire d'Etudes Mécaniques des Assemblages (FRE 2481), Université de Versailles/Saint-Quentin-en-Yvelines
45 Av. des Etats-Unis, 78035 Versailles Cedex, France
e-mail: corrado.maurini@meca.uvsq.fr, joel.pouget@meca.uvsq.fr

† Dipartimento di Ingegneria Strutturale e Geotecnica, Università di Roma "La Sapienza
via Eudossiana 18, 00184 Roma, Italy
e-mail: francesco.dellisola@uniroma1.it

Keywords: Euler-Bernoulli, Mixed Variational Principle, Piezoelectric, Laminates, Beams

Abstract. *Beam models of piezoelectric laminates derived from three-dimensional theories by assuming either the plain-stress or the plain-strain conditions in the beam axis-thickness plane can introduce significant errors in the estimate of the beam constitutive coefficients. In this paper a coupled Euler-Bernoulli-like model including 3D effects through a mixed variational formulation is discussed. We report the results of numerical and experimental tests which validate the approach and show the limit of standard modelling techniques.*

1 INTRODUCTION

Many structural systems with actuating and sensing capabilities include slender beam-shaped piezoelectric laminates. Piezoelectric sandwich and bimorph beams are very often used as part of sensors and actuators and micro-resonators. Moreover, piezoelectric laminated beams are encountered in applications to structural control. Actively or passively shunted surface-bonded piezoelectric patches provide an efficient mean for vibration damping or health monitoring. Common configurations exploit the bending-electric coupling obtained with sandwich and bimorph beams including layers of thickness-polarized piezoelectric ceramics (see Figure 1).

Computationally efficient one-dimensional models of this class of smart structures are very useful in the design process and they are widely adopted in the engineering practice. The actuation effect obtained in elastic beams with surface bonded or embedded piezoelectric patches was analyzed by Crawley and Anderson [1]. They adopted the induced-strain approach, where piezoelectric strains are treated in analogy to thermal effects. Many applications demand fully coupled models including explicitly both mechanical and electric degrees-of-freedom. Among

others, electromechanical behavior of piezoelectric bimorph and sandwich beams was studied by [2, 3, 4, 5, 6, 7]. As underlined in [8] and [9], a careful electromechanical modelling is required also for ensuring a correct estimate of purely mechanical properties. Euler-Bernoulli-like models are the most commonly used, especially in control applications. But several refined interesting approaches including higher order effects in sheareable and layerwise models are proposed [10, 11].

The overwhelming majority of works on beam modelling of piezoelectric laminates assume, as first move, that the 3D model can be reduced to a 2D one by concentrating on the analysis in the axis-thickness plane. This is usually done by assuming a plane-stress condition, which is motivated through reasoning inherited by elementary beam theory, as explicitly reported in [4][1]. Other authors eliminate the transversal (width) direction by accepting the plane strain hypothesis (see e.g. [11]). Unfortunately the real stress-strain state of thickness-polarized piezoelectric laminates is more complex. Neither the plane stress nor the plane strain conditions are physically grounded. In thickness-polarized piezoelectric layers, the deformations induced by an applied electric potential are isotropic in the $\mathbf{e}_1 - \mathbf{e}_2$ plane. On the contrary, in elastic layers, an axial extension is usually associated to a transverse shrinking by the classical Poisson effect. When elastic and piezoelectric layers are bonded together, these different behaviors must be reconciled. Hence, non-negligible transverse stresses T_{22} arise and non-trivial sectional deformations appears.

The influence of 3D effects was underlined by Beckert and Pfundtner [12] in their analysis of the strain transfer from a piezoelectric patch to an elastic beam. Complex sectional warping effects are included also in some advanced modelling techniques used for composite beam-like structures as airplane-wing and helicopter-blades, where an accurate prediction of the torsion-bending-extesion coupling is important. Chopra and co-workers [13, 14] underline the influence of transverse bending considering skewed piezoelectric transducers in torsion-bending-extension coupled actuation. They propose a Vlasov-like beam model for thin-walled beams which includes the effect of cross-sectional warping. But the analysis was limited again to the actuation function (uncoupled model) and does not include the influence of the induced potential. Moreover, the model is more complex that the Euler-Bernoulli one since it introduces several additional mechanical degrees of freedom. More accurate semi-analytical modelling techniques [15, 16] exploit a variational asymptotic approach to split up the 3D problem in a 2D cross-sectional model and a 1D axial model. The cross-sectional problem is solved numerically and its solution provides the constitutive behavior of the axial problem. They are applied to piezoelectric composite by [17] and [18].

The literature review of beam models of piezoelectric laminates shows that the effects of sectional warping are not fully understood and that efficient and accurate coupled Euler-Bernoulli models are not available. For this reason, beam-shaped piezoelectric laminates are often modelled either by 3D finite elements or 2D plate models. In this paper, we develop and validate

[1] From [4]: "Stresses T_{33} and T_{22} can be considered of the order of any loading forces possibly imposed in the x_3- and x_2-directions. Since in our structure we are not considering significant loading forces in these directions, stresses T_{33} and T_{22} can be disregarded, $T_{33} = T_{22} = 0$"

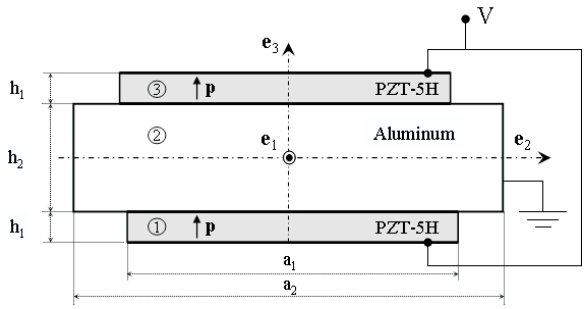

Figure 1. Cross-section of a sandwich piezoelectric beam. The two piezoelectric layers are polarized along the same direction ($\mathbf{p}$). Their electrodes are connected in parallel and in counter-phase to obtain a bending-electric coupling. A bimorph bender is obtained when $h_2 = 0$.

the results recently presented by the authors in [19] and [20], where a coupled Euler-Bernoulli model including the effect of cross sectional deformation is developed. The model exploits a mixed variational approach to account for the primary effects of cross-sectional in-plane warping and induced electric potential, without introducing additional degrees-of-freedom.

The paper is organized as follows. Section 2 recalls the basic hypotheses and the fundamental equations of the proposed beam model, as presented in [20]. Section 3 presents numerical comparisons with 3D finite element results and standard beam models for the case of a cantilever bimorph beam. Section 4 reports comparisons with experimental results obtained for a beam with a pair of surface-bonded piezoelectric transducer in sandwich configurations. Section 5 is left for conclusions.

2 ENHANCED EULER-BERNOULLI MODEL

This section briefly presents the basic hypotheses and the governing equations of an Euler-Bernoulli-like model of piezoelectric laminates including the effect of *cross-sectional in-plane warping* and of the *induced electric potential*. The model is obtained from 3D piezoelectricity by using a deductive approach based on an Hellinger-Reissner-like mixed variational formulation. The interested reader can found further details in [19, 20].

2.1 Geometry

Referring to the reference frame reported in Figure 1, where $\mathbf{e}_1$ is parallel to the beam axis, the model concentrates only plane bending in the $\mathbf{e}_1 - \mathbf{e}_2$ plane of a straight-axis beam. The axial $(\mathbf{e}_1)$ and transverse $(\mathbf{e}_3)$ deflections of the beam axis $\mathcal{A}$ are denoted by $u(x)$ and $w(x)$, respectively, where x is a generic point on $\mathcal{A}$. Assuming a fully linear theory, $u'(x)$ and $w''(x)$ represent the axis extension and curvature. Each layer is supposed to be homogeneous and transversely isotropic with respect to the thickness direction $\mathbf{e}_3$, which coincides with the polarization axis of the piezoelectric ceramics. The layers' thicknesses and widths are denoted by h_i and a_i, respectively. The electrodes of different layers are connected in parallel, either in phase

or in counter phase, and the whole beam is electrically accessible only through two external electric terminals.

2.2 Mixed variational formulation

Let $\mathcal{B}$ be a piezoelectric body with boundary $\partial\mathcal{B}$ and loaded with volume force $\mathbf{b}$ on $\mathcal{B}$, surface forces $\mathbf{f}_0$ on $\partial_{\mathbf{f}}\mathcal{B}$, surface charges q_0 on $\partial_{\mathbf{f}}\mathcal{B}$. Moreover, let be

$$\mathcal{F}(\mathbf{T},\mathbf{D}) = \frac{1}{2}\mathbf{s}^D\mathbf{T}\cdot\mathbf{T} - \frac{1}{2}\beta^T\mathbf{D}\cdot\mathbf{D} + \mathbf{g}\mathbf{T}\cdot\mathbf{D} \tag{1}$$

a piezoelectric energy density, where $\mathbf{T}$ and $\mathbf{D}$ are the symmetric Cauchy stress tensor and the electric displacement vector; $\left(\mathbf{s}^D, \beta^T, \mathbf{g}\right)$ are the constitutive tensors of linear piezoelectric materials. Moreover, let be $(\mathbf{u}, \mathbf{S}(\mathbf{u}))$ and $(\varphi, \mathbf{E}(\varphi))$ pairs of compatible mechanical displacement and strain fields**,** and compatible electric potential and electric fields, which respect the essential boundary conditions prescribed on $\mathbf{u}$ and φ. A weak formulation of the electromechanical *balance* and *constitutive equations* of a piezoelectric body is obtained by looking for the stationary point of the following mixed functional over the functional space of regular $(\mathbf{u},\varphi, \mathbf{T}, \mathbf{D})$:

$$\Theta[\mathbf{u},\varphi,\mathbf{T},\mathbf{D}] = \int_{\mathcal{B}} \left(\mathcal{F}(\mathbf{T},\mathbf{D}) - \mathbf{T}\cdot\mathbf{S}(\mathbf{u}) + \mathbf{D}\cdot\mathbf{E}(\varphi) + \mathbf{b}\cdot\mathbf{u}\right) d\mathcal{B} + \int_{\partial_{\mathbf{f}}\mathcal{B}} \mathbf{f}_0\cdot\mathbf{u}\, d\mathcal{S} + \int_{\partial_q\mathcal{B}} q_0\varphi\, d\mathcal{S} \tag{2}$$

The mixed variational principle provides a weak formulation of the beam balance and constitutive equations, where electromechanical balance equations are tested by the mechanical displacements and the electric potential, the corresponding constitutive equations by the mechanical stresses and the electric displacement.

The mixed variational formulation is particularly useful in structural modelling [21]. In standard variational formulations one introduces hypotheses on the generalized kinematic fields $(\mathbf{u},\varphi)$, but the associated force-like fields $(\mathbf{T},\mathbf{D})$ are automatically determined by the 3D constitutive equations. The mixed setting presented above allows to specify also the distribution of force-like fields by introducing all what is known a priori on the distribution of $(\mathbf{T},\mathbf{D})$, independently of the kinematical prescriptions. In particular, it allows to refine standard beam and plate theories without introducing additional degrees-of-freedom.

2.3 Hypotheses

The beam model is derived by the mixed variational functional (2), by assuming the following a priori hypotheses on the electromechanical field distribution:

(i) *Mechanical displacement.* Basic equivalent-single-layer Euler-Bernoulli kinematics:

$$\mathbf{u}(x,y,z) = \left(u(x) - zw'(x)\right)\mathbf{e}_1 + w(x)\mathbf{e}_3, \tag{3}$$

(ii) *Electric potential.* Layerwise linear distribution of the electric potential, which, when the different layers are electrically interconnected in parallel (either in-phase, $\omega_i = 1$, or in

counter-phase, $\omega_i = -1$), is given by the following expression

$$\varphi(x,y,z) = \left(\frac{1}{2} + \omega_i \frac{z_i}{h_i}\right) V, \tag{4}$$

where V is the electric potential difference across the two external electric terminals.

(iii) *Mechanical stress*. A stress tensor composed of axial and transverse normal stresses, having constant ($\sigma_{\alpha,i}$) and linear ($\zeta_{\alpha,i}$) contributions through the thickness of each layer,

$$\mathbf{T}(x,y,z) = \left(\sigma_{1,i}(x,y) - z_i\zeta_{1,i}(x,y)\right)(\mathbf{e}_1 \otimes \mathbf{e}_1) + \left(\sigma_{2,i}(x,y) - z_i\zeta_{2,i}(x,y)\right)(\mathbf{e}_2 \otimes \mathbf{e}_2), \tag{5}$$

and respecting the following conditions on the through-the-thickness force (n_2) and moment (m_2) resultants of transverse (chordwise) stresses

$$\begin{cases} n_2(x,y) = \displaystyle\sum_{i\in\mathcal{I}(x,y)} \int_{\mathcal{I}_i} \mathbf{T}(x,y,z)\mathbf{e}_2 \cdot \mathbf{e}_2 dz = 0 \\ m_2(x,y) = \displaystyle\sum_{i\in\mathcal{I}(x,y)} \int_{\mathcal{I}_i} -z\mathbf{T}(x,y,z)\mathbf{e}_2 \cdot \mathbf{e}_2 dz = 0 \end{cases} \tag{6}$$

(iv) *Electric displacement*. Layerwise constant distribution along the thickness direction:

$$\mathbf{D}(x,y,z) = D_i(x,y)\mathbf{e}_3, \tag{7}$$

where $D_i(x,y)$ is the function giving the $\mathbf{e}_3$ component of the electric displacement in the i-th layer.

As results of the machinery of the adopted mixed variational formulation, the hypotheses above lead to a model where:

- Each cross-section moves remaining plane and orthogonal to the beam axis (Euler-Bernoulli hypothesis).
- Each cross-section deforms in its own plane (in-plane warping) with chordwise bending and thickness distension, so as to respect conditions (5-6).
- Shear effects are neglected.
- In each piezoelectric layer the electric displacement is oriented along the thickness and its module is constant in the thickness coordinate.
- In each piezoelectric layer the electric potential has a through-the-thickness quadratic distribution, including the induced electric potential. Only its linear part, determined by the potential difference across the electrodes, appears explicitly in the beam equations. The quadratic part is automatically determined as a function of the flexural strains, so as to assure that condition (7), i.e. that the electric displacement is constant (see [8, 9]).

2.4 Beam Governing Equations

The beam balance equations, natural boundary conditions and constitutive equations are found as Euler equations of the mixed functional (2) when the electromechanical fields are constrained

to verify conditions (i-iv). In particular, the conditions (6) on the transverse stress are conveniently introduced by the Lagrange multiplier method, as shown in [20]. The corresponding Lagrange multipliers represent the generalized sectional deformations associated to chordwise extension and bending.

The governing equations appear in the format of a standard Euler-Bernoulli model, with an additional electric degree of freedom to describe the electric potential difference at the electric terminals. In each regular beam segment they are composed of the following elements:

- The *equilibrium equations* for the axial force $N_1(x)$, the bending moment $M_1(x)$, and the total charge at the electric terminal $Q = \int_{\mathcal{A}} q(x)dx$, $q(x)$ being the electric charge per unit line:
$$\begin{cases} b_N(x) + N_1'(x) = 0 \\ b_M'(x) - b_T(x) + M_1''(x) = 0 \\ \int_{\mathcal{A}} q(x)dx + \bar{Q} = 0 \end{cases}, \tag{8}$$
where the external actions are represented by the axial $b_N(x)$ and transversal $b_T(x)$ force per unit line, the bending moment per unit line $b_M(x)$ and the total charge $\bar{Q}$ prescribed at the electric terminals. Inertial actions can be included as suitable constitutive prescription of $b_N(x)$, $b_T(x)$, and $b_M(x)$; shunting electric networks are modelled as constitutive prescription of $\bar{Q}$ in terms of the potential V.
- The *natural boundary conditions*, which are found by the following variational equations
$$\left[\left(N_1 - \bar{N}\right)\delta u\right]_{\partial\mathcal{A}} = 0, \tag{9a}$$
$$\left[\left(M_1 - \bar{M}\right)\delta w' + \left(\bar{T} + M_1' + b_M\right)\delta w\right]_{\partial\mathcal{A}} = 0, \tag{9b}$$
where $(\delta u, \delta w, \delta w')$ are admissible variations of the kinematical fields respecting the essential boundary conditions; $\bar{N}, \bar{T}, \bar{M}$ are applied axial force, transverse force, and bending moment at the boundaries.
- the piezoelectric *constitutive equations* at the beam level, which appear in the form:
$$\begin{bmatrix} N_1 \\ M_1 \\ q \end{bmatrix} = \begin{bmatrix} k_{Nu} & k_{Nw} & e_{NV} \\ k_{Nw} & k_{Mw} & -e_{MV} \\ -e_{NV} & e_{MV} & \varepsilon_{qV} \end{bmatrix} \begin{bmatrix} u' \\ w'' \\ V \end{bmatrix}. \tag{10}$$

The proposed model provides accurate expressions of the constitutive coefficients appearing in (10), by including the effect of cross-sectional warping and induced electric potential.

2.5 Electromechanical constitutive equations

The expressions giving the constitutive coefficients appearing in (10) are found after simple manipulations of the Euler-equations of the mixed variational problem under the hypotheses (3-7). We refer to [20] for the detailed derivation in the case of piezoelectric laminated beams composed of an arbitrary number of transversely isotropic layers. In the following, we report only the formulas found for two specific layer configurations which are commonly encountered in applications: piezoelectric sandwich and piezoelectric bimorph.

2.5.1 Piezoelectric sandwich

In the piezoelectric sandwich beam characterized by the cross section in Figure 1, because of the material and geometric symmetry, beam extension and bending are decoupled. Moreover, due to the electric interconnection between the two piezoelectric layers, also extensional and electric equations are uncoupled. Hence, the constitutive equations (10) for the bending moment, M_1, and the electric charge per unit line, q, assume the following simplified form:

$$\left[\begin{array}{c} M_1 \\ q \end{array}\right] = \left[\begin{array}{cc} k_{Mw} & -e_{MV} \\ e_{MV} & \varepsilon_{qV} \end{array}\right] \left[\begin{array}{c} w'' \\ V \end{array}\right] \tag{11}$$

and the bending-electric problem can be solved separately from the extensional one. The following expressions for the constitutive coefficients in equations (11) are found

$$k_{Mw} = a_1 K_{11}\left(1 - \frac{K_{12}^2}{K_{11}^2}\right) + (a_2 - a_1)\,\frac{1}{12} h_2^3 \tilde{c}_{11}\left(1-\nu^2\right), \tag{12a}$$

$$e_{MV} = a_1 \tilde{e}_{31}\,(h_1 + h_2)\left(1 - \frac{K_{12}}{K_{11}}\right), \tag{12b}$$

$$\varepsilon_{qV} = \frac{2a_1 \tilde{\epsilon}_{33}^S}{h_1} + \frac{a_1\left(\tilde{e}_{31}\,(h_1+h_2)\right)^2}{K_{11}}, \tag{12c}$$

where the stiffness parameters K_{11}, K_{12} are defined as follows (see also Table 1)

$$K_{\alpha\beta} = \frac{\tilde{c}_{\alpha\beta}^E h_1^3}{12}\left(6\left(1+\frac{h_2}{h_1}\right)^2 + 2\frac{\tilde{c}_{\alpha\beta}^D}{\tilde{c}_{\alpha\beta}^E} + \frac{\tilde{c}_{\alpha\beta}}{\tilde{c}_{\alpha\beta}^E}\frac{h_2^3}{h_1^3}\right). \tag{13}$$

2.5.2 Two-layer bimorph

The constitutive coefficients for the bimorph bender made of two piezoelectric layers connected in parallel and in counter phase are obtained from expressions (12) by letting the thickness of the elastic layer (h_2) go to zero:

$$k_{Mw}^{(b)} = \frac{4(2+\gamma^2+2\nu^E)}{(4+\gamma^2)(1+\nu^E)}\frac{a_1 h_1^3 Y^E}{3}, \tag{14a}$$

$$e_{MV}^{(b)} = \frac{4}{4+\gamma^2} a_1 d_{31} Y^E h_1, \tag{14b}$$

$$\varepsilon_{qV}^{(b)} = \frac{2a_1}{h_1 \beta_{33}^T}\left(1 - d_{31}^2 Y^E \beta_{33}^T \frac{5+2\gamma^2-3\nu^E}{(4+\gamma^2)\,(1-\nu^E)}\right). \tag{14c}$$

2.6 Transverse (chordwise) deformations

In Euler-Bernoulli models, through-the-thickness constant and linear contributions to axial normal strains, say ε_1, are given by axis extension $u'(x)$ and axis curvature $w''(x)$, respectively:

$$\varepsilon_1(x,z) = u'(x) - z w''(x) \tag{15}$$

Piezoelectric Layers		Elastic Layers
$\tilde{c}^E_{11}=\frac{1}{s^E_{11}}\frac{1}{1-(\nu^E)^2}$	$\tilde{c}^D_{11}=\tilde{c}^E_{11}\left(1+\gamma^2\right)$	$\tilde{c}_{11}=\frac{1}{s_{11}}\frac{1}{1-\nu^2}$
$\tilde{c}^E_{12}=\nu^E\tilde{c}^E_{11}$	$\tilde{c}^D_{12}=\tilde{c}^E_{12}\left(1+\gamma^2/\nu^E\right)$	$\tilde{c}_{12}=\nu\tilde{c}_{11}$
$\tilde{e}_{31}=\frac{d_{31}}{s^E_{11}(1-\nu^E)}$	$\tilde{\epsilon}^S_{33}=\frac{1}{\beta^T_{33}}\left(1-\frac{2\beta^T_{33}d^2_{31}}{s^E_{11}(1-\nu^E)}\right)$	$\nu=-s_{12}/s_{11}$
$\nu^E=-s^E_{12}/s^E_{11}$	$\gamma=\sqrt{\tilde{e}^2_{31}/\left(\tilde{c}^E_{11}\tilde{\epsilon}^S_{33}\right)}$	

Table 1. Constitutive coefficients of the piezoelectric and elastic layers in the plane stress condition ($T_{33}=0$) .

The present model takes into account also in-plane deformations of the beam cross-sections. In particular through-the-thickness constant and linear contributions of chordwise normal strains are introduced as Lagrange multipliers to enforce the conditions (6). Being $\lambda(x,y)$ the Lagrange multiplier associated to the conditions of vanish transverse stress resultant ($n_2(x,y)=0$), $\mu(x,y)$ the one associated to the conditions of vanish moment resultant ($m_2(x,y)=0$), the transverse normal strains are given by

$$\varepsilon_2(x,y,z)=\lambda(x,y)-z\mu(x,y). \tag{16}$$

Thus transverse deformations are determined as a function of the axial fields ($u'(x), w''(x), V$) so as to ensure the free-transverse bending conditions (6) and relations of the following form are found

$$\left[\begin{array}{c}\lambda\\ \mu\end{array}\right]=\left[\begin{array}{cc}\alpha_{\lambda u} & \alpha_{\lambda w}\\ \alpha_{\lambda w} & \alpha_{\mu u}\end{array}\right]\left[\begin{array}{c}u'(x)\\ w''(x)\end{array}\right]+\left[\begin{array}{c}\alpha_{\lambda V}\\ \alpha_{\mu V}\end{array}\right]V. \tag{17}$$

For the piezoelectric sandwich beam, the transverse deformations are given by (it is assumed that $u'(x)=0$)

$$\varepsilon_2(x,y,z)=\left\{\begin{array}{ll}-z\frac{K_{12}}{K_{11}}w''(x)-z\frac{\tilde{e}_{31}(h_1+h_2)}{K_{11}}V, & y\in\left(-\frac{a_1}{2},-\frac{a_1}{2}\right)\\ -z\tilde{c}_{12}/\tilde{c}_{11}w''(x), & y\in\left(-\frac{a_2}{2},-\frac{a_1}{2}\right)\cup\left(\frac{a_1}{2},\frac{a_2}{2}\right)\end{array}\right. \tag{18}$$

The introduction of transverse normal deformation in the framework of an Euler-Bernoulli model is a main improvement with respect to standard modelling techniques. Standard beam models assume either the plane strain or the plane stress condition in the axis-thickness plane. In the plane strain case, transverse (chordwise) strains are null. In the plane stress case transverse normal strains are determined to enforce the conditions of pointwise vanishing transverse stress and different layers are left free to slide on each other, without respecting the bonding conditions in the transverse direction (see Figure 2) [19, 20]. Here and henceforth we refer to the model assuming pointwise null transverse normal stresses as *NS model*, the model assuming null transverse deformation as *ND model*, and the model presented above and introducing the conditions (6) of vanishing stress resultants as *NSR model.*

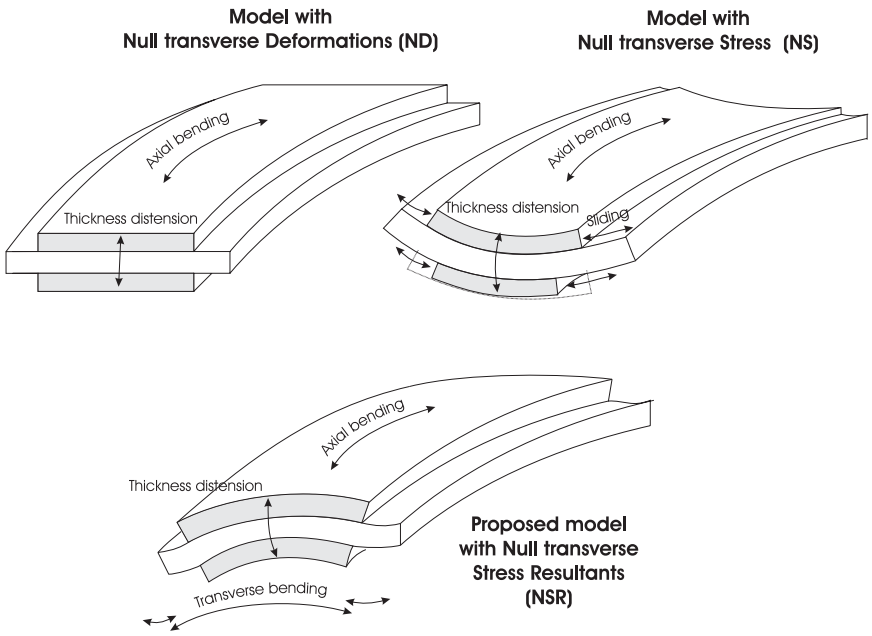

Figure 2. Cross-sectional deformations in models assuming null transverse deformations (ND), null transverse strain (NS), and the present model assuming null stress resultants (NSR).

3 CANTILEVER BIMORPH: NUMERICAL COMPARISONS WITH 3D FEM.

3.1 Analytic expressions of the global constitutive equations

Let us consider a cantilever bimorph beam as shown in Figure 3. The tip-displacement δ and total electric charge Q are expressed as a function of static applied voltage V and tip-force F as follows

$$\left[\begin{array}{c} \delta \\ Q \end{array} \right] = \left[\begin{array}{cc} f_{\delta F} & f_{\delta V} \\ f_{\delta V} & f_{QV} \end{array} \right] \left[\begin{array}{c} F \\ V \end{array} \right]. \tag{19}$$

When assuming the Euler-Bernoulli beam model, the coefficients appearing in equations (19) are found by solving the simple boundary value problem for the electromechanical system:

$$f_{\delta F} = \frac{l^3}{3k_{Mw}},\ f_{\delta V} = -\frac{e_{MV} l^2}{2k_{Mw}},\ f_{QV} = l\varepsilon_{qV}\left(1 + \frac{e_{MV}^2}{k_{Mw}\varepsilon_{qV}}\right) \tag{20}$$

Depending on the hypotheses introduced in the beam model, the constitutive parameters (k_{Mw}, e_{MV}, ε_{qV}) can have different expressions. Smits et al. [3] proposed a model assuming uniaxial stress ($T_{22} = T_{33} = 0$) and a linear distribution of the electric potential through the thickness of each layer. Similar approaches are followed in [2, 3, 6, 7]. Table 2 compares the analytic expressions for ($f_{\delta F},\ f_{\delta V},\ f_{QV}$) found by Smits, to those obtained in a model in plane-stress but accounting for the quadratic contribution of the electric potential (NS), and to those found with

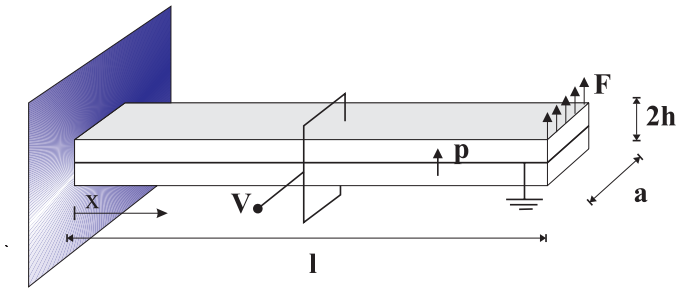

Figure 3. Cantilever bimorph with applied voltage and tip force.

	Smits et al. [3]	NS	Present
$f_{\delta F}$	$\frac{3s_{11}^E l^2}{2ah^3}$	$\frac{2l^3}{ah^3 Y_E(4+\gamma^2)}$	$\frac{l^3}{4ah^3 Y_E}\frac{(4+\gamma^2)(1+\nu^E)}{\gamma^2+2(1+\nu^E)}$
$f_{\delta V}$	$\frac{-3d_{31}l^2}{4h^2}$	$-\frac{3d_{31}l^2}{h^2(4+\gamma^2)}$	$-\frac{3d_{31}l^2}{2h^2}\left(\frac{1+\nu^E}{\gamma^2+2(1+\nu^E)}\right)$
f_{QV}	$\frac{2al}{\beta_{33}^T}\left(1-\frac{\beta_{33}^T d_{31}}{4s_{11}^E}\right)$	$\frac{2al}{h\beta_{33}^T}\left(1-d_{31}^2 Y^E \beta_{33}^T \frac{(1+\gamma^2)}{(4+\gamma^2)}\right)$	$\frac{2al}{h\beta_{33}^T}\left(1-\frac{d_{31}^2 Y^E \beta_{33}^T (2\gamma^2+1+\nu^E)}{(1-\nu^E)(\gamma^2+2(1+\nu^E))}\right)$

Table 2. Analytic expressions of the coefficients appearing in the constitutive equations of a piezoelectric bimorph (Eqn. (19)). Comparisons between the different beam models: Smits et al. [3] assumes uniaxial stress and neglects the induced potential; (NS) assumes uniaxial stress but includes the effect of the induced potential; the present model includes assumes transverse stress resultants and includes the effect of the induced potential.

the expressions (14a) associated to the present model assuming null transverse stress resultants.

3.2 3D Finite Element results

Results of 3D finite element simulations provide a numerical reference for the constiutive coefficients reported in Table 2 and are useful also for analyze the influence of the *boundary effects*. Due to the 3D effects associated to the clamping conditions beam models are expected to be accurate only for sufficiently high aspect ratios (length to cross-sectional diameter).

The FE simulations were performed by using the commercial code Ansys 8.0. The basic brick-shaped SOLID5 element with 10 nodes and 4 d.o.f.'s per node (displacement vector and electric potential) was adopted. After refinement essays, a mapped mesh composed of 5 elements through the thickness of each layer and 8 elements through the width was adopted. The element length in the axial direction was chosen as a function of the total beam length to fix the element length to thickness aspect ratio to 2.5. For example, for a beam having $a/h = l/a = 10$, the mesh is composed of 16000 elements. The two layers are assumed to be perfectly bonded and the mechanical properties of the electrodes are neglected. The coefficients appearing in (19) are estimated by detecting the tip displacements δ and the total charge at the electrodes Q for two different loading conditions: (i) applied potential for null mechanical forcing; (ii) applied

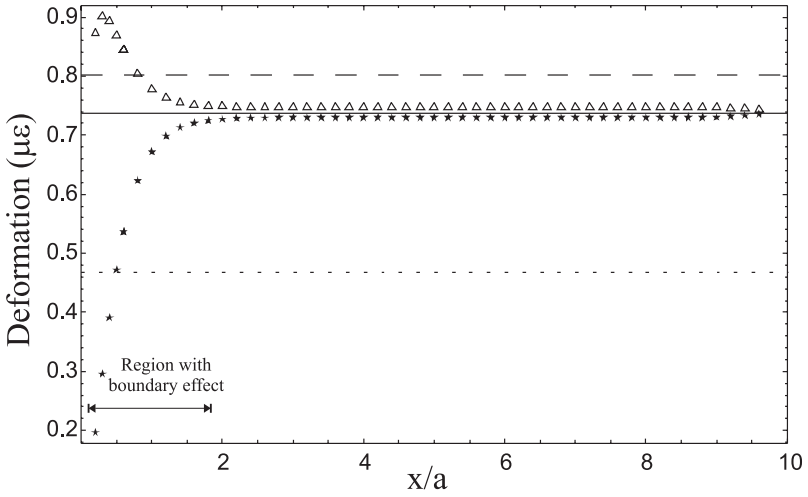

Figure 4. Axial and transverse strains at the center of the upper surface of the piezoelectric bimorph as a functions of the axial coordinate x. Present model: ε_1 and ε_2 coincide $(-)$; model with null transverse stress (NS): ε_1 $(--)$ and ε_2 $(\cdots)$; FEM 3D: ε_1 $(\triangle)$ and ε_2 $(\star)$.

Elastic Layers	
$Y = 1/s_{11} = 69 \times 10^9\,\mathrm{N}\,/\,\mathrm{m}^2$	$\nu = -s_{11}/s_{12} = 0.33$
Piezoelectric Layers	
$Y^E = 1/s^E_{11} = 62 \times 10^9\,\mathrm{N}\,/\,\mathrm{m}^2$	$\nu^E = -s^E_{11}/s^E_{12} = 0.31$
$d_{31} = -320 \times 10^{-12}\,\mathrm{m}\,/\,\mathrm{V}$	$\beta^T_{33} = 1/\varepsilon^T_{33} = 2.97 \times 10^7\,\mathrm{m}\,/\,\mathrm{F}$

Table 3. Constitutive properties of the considered piezoelectric (PZT-5H) and elastic (aluminum) materials.

uniform distribution of shear forces at the beam free-end, under the short-circuit condition. The numerical simulations assumes $a = 10h$, $h = 0.5\,\mathrm{mm}$ and the material data reported in Table 3. The full 3D constitutive equations used for the finite element calculations coincide with those reported in [20]. The results obtained for beam having different length-to-width aspect ratios are reported in Tables 4-6 and compared with the corresponding estimates given by the different beam models. For applied electric potential, Figure 4 reports also the distributions of axial and transverse strains at the center line of the upper surface of the upper piezoelectric transducer as function of the axial coordinate. The axial ($\varepsilon_1(x, 0, h)$) and transverse ($\varepsilon_2(x, 0, h)$) strains found with a FE simulation are compared to those obtained with the present model and the NS model.

3.3 Comments

The analysis of the numerical results shows that:

- For slender beams ($l/a \geq 10$) the one-dimensional models are supposed to be in good

Equivalent Capacitance (f_{QV})				
l/a	3DFEM	Smits	NS	Present
	nF	$\%\, diff.$	$\%\, diff.$	$\%\, diff.$
2	5.122	$+25.27\%$	$+22.29\%$	$+1.03\%$
4	10.36	$+23.84\%$	$+20.89\%$	-0.13%
6	15.56	$+23.40\%$	$+20.38\%$	-0.48%
8	20.83	$+23.19\%$	$+20.17\%$	-0.65%
10	26.07	$+23.06\%$	$+20.05\%$	-0.76%
20	52.25	$+22.80\%$	$+19.80\%$	-0.96%

Table 4. Electric charge at the electrodes for applied unit potential difference and null tip force (i.e. equivalent piezoelectric capacitance at constant force) of a piezoelectric bimorph as a function of the aspect ratio l/a (length over width). Comparisons between results from different beam models and 3D FE simulations (Smits et al. [3]: null transverse stress without induced potential; (NS): null transverse stress with induced potential; Present (NSR): null transverse stress resultants with induced electric potential)

Compliance ($f_{\delta F}$)				
l/a	3DFEM	Smits	NS	Present
	$\mu\mathrm{m}\,/\,\mathrm{N}$	$\%\, diff.$	$\%\, diff.$	$\%\, diff.$
2	11.02	17.04%	-2.25%	7.69%
4	91.03	13.39%	-5.30%	4.33%
6	311.4	11.88%	-6.56%	2.95%
8	743.4	11.08%	-7.23%	2.20%
10	1456	10.59%	-7.647%	1.75%
20	11770	9.57%	-8.49%	0.82%

Table 5. Tip displacement for applied unit tip force under the short-circuit condition (i.e. mechanical compliance at constant potential) of a piezoelectric bimorph as a function of the aspect ratio l/a (length over width). Comparisons between results from different beam models and 3D FE simulations

Piezoelectric Coupling ($f_{\delta V}$)				
l/a	3DFEM	Smits	NS	Present
	$\mu\mathrm{m}\,/\,\mathrm{V}$	$\%\, diff.$	$\%\, diff.$	$\%\, diff.$
2	0.0785	22.10%	2.01%	-6.13%
4	0.3090	23.80%	3.24%	-4.80%
6	0.6907	25.09%	4.47%	-3.87%
8	1.221	25.81%	5.07%	-3.32%
10	1.900	26.28%	5.47%	-2.96%
20	7.539	26.33%	5.63%	-2.15%

Table 6. Tip displacement for unit potential difference and null tip force (piezoelectric coupling coefficient) of a piezoelectric bimorph as a function of the aspect ratio l/a (length over width). Comparisons between results from different beam models and 3D FE simulations

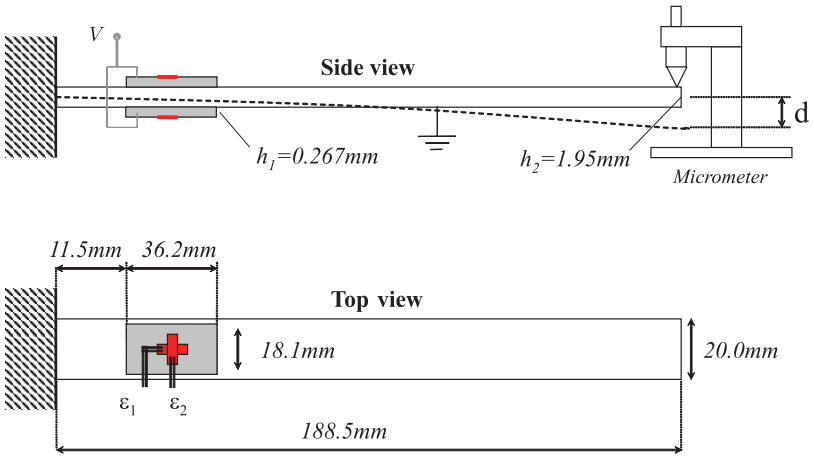

Figure 5. Experimental set-up for strain analysis. Two two-element 90° tee rosette were positioned at the center of each transducer. The strain gages capture both axial and transverse strains and are connected to detect only anti-symmetric bending strains.

agreement with the 3D theory. However, only the present NSR model gives good results for all the electromechanical coefficients appearing in equations (11). In models assuming the uniaxial stress condition, the equivalent piezoelectric capacitance presents substantial errors. The comparison between the NS model and the Smits' model shows that the introduction of the induced potential implies a reduction of the mechanical stiffness and piezoelectric coupling. But, while introducing the induced potential ameliorates the estimate of the coupling coefficient, it leaves approximately the same error on the mechanical stiffness, changing only the sign (from an overestimate to a underestimate).

- For short beams, the boundary effects have an influence. In particular, the clamping condition, blocking the sectional deformations, leads to a stiffening phenomenon and to an increase of the axial-electric coupling. In the present model, as expected for a beam theory, the lower is the slender ratio l/a, the lower is the model accuracy (the errors being still under 5% for $l/a = 4$). On the contrary, the NS model takes advantage of the boundary stiffening and the relative errors on the compliance and the coupling coefficient becomes smaller for shorter beams. But this is due more to a cancellation of error effect than to an effective catching of the distribution of the electromechanical 3D energy. This is clearly shown by the errors on the piezoelectric capacitance, which increase.

The present results on the numerical validation of the beam model complete those presented in [20], where the influence of boundary effects was not analyzed and only a comparison of the local constitutive equations in the form (11) is given.

4 EXPERIMENTS

4.1 Static strain analysis of a beam with piezoelectric patches

4.1.1 Experimental set-up

A pair of identical piezoelectric transducers (Piezo-System T110-H4E-602) were bonded on a cantilever aluminum beam (Al6061-T6) as shown in Figure 5. The transducers are electrically connected in parallel and counter-phase, so as to form, with the aluminum layer, a sandwich beam with electric-bending coupling. The single piezoelectric transducer is made of a layer of thickness-polarized piezoelectric ceramic (PZT-5H) having the upper and lower surfaces electroded by a nickel film. The transducers were bonded on the beam using a two-component structural epoxy. The electric contact between the inner electrode of each transducer and the grounded beam was achieved by applying a small spot of electrically conductive adhesive at the central region of the piezoelectric transducer, where, as shown by stress-transfer analysis [1], interfacial stresses are low. Each transducer was instrumented with a strain gage CEA-06-062UT-350, bonded at the center of the piezoelectric elements with proper adhesive. This is a two-element 90° tee rosette and it was positioned to measure longitudinal and transverse strains. The strain gages on the lower and the upper piezoelectric transducers were connected in the half-bridge configuration so as to sense only antisymmetric bending strains. Two different signal conditioners HBM Scout 55 were used as Wheatstone bridges and signal amplifiers. The axial and transverse strains were measured for two different loadings: a) a voltage difference V applied between the grounded beam and the electric terminal of the piezoelectric sandwich; b) a displacement imposed at the tip of the beam. In the first case, the voltage was applied through an amplifier suitably designed for the high-impedance of the piezoelectric transducers and the beam was left free to deform. In the second case, a controlled static tip displacement was imposed by a micrometer and the pair of piezoelectric transducers was shorted to ground.

4.1.2 Results

Applied voltage Figure 6 reports the axial and transverse strains at the surfaces of the piezoelectric transducers measured when different voltages V are imposed at the piezoelectric pair. Two different sets of measurements were taken. The first set is in *static condition*, the second set is in *quasi-static conditions*. Static tests are affected by the well-known *drift* phenomenon, i.e. a slow increase of the strain with time after the application of the DC field [14]. In the present tests, each strain value was recorded after holding the corresponding DC voltage for about one minute. The voltage where increased from 0 to 45 Volt with steps of 5 Volt and then decreased again to 0 Volt. Quasi-static[2] tests were performed by applying harmonic voltage at the frequency of $6Hz$, for 16 different peak-to-peak amplitudes in the range between 3.4 and 32.8 Volt. The strain values induced by these voltage levels are quite small (in the range $1 \div 50\mu\varepsilon$) and at the limit of the sensitivity of strain gauges and the related measurement chain.

[2]The first resonance frequency of the beam is at $47.3\,\mathrm{Hz}$.

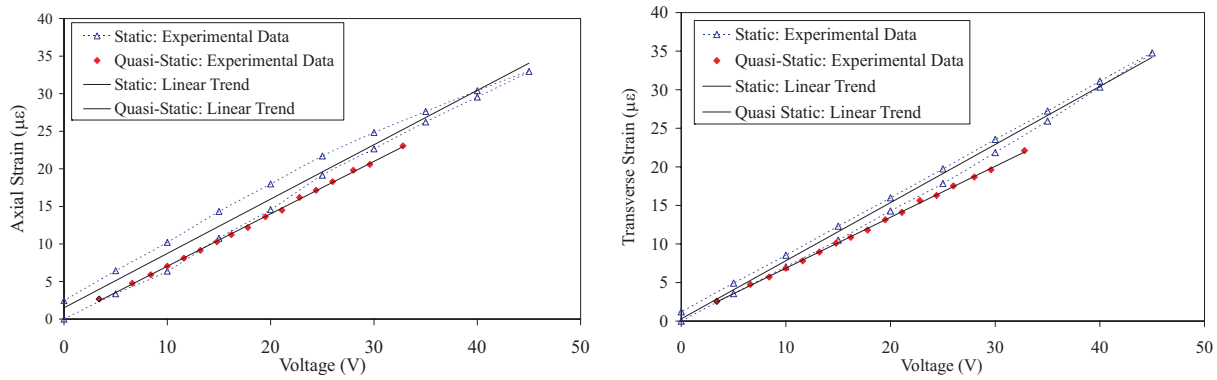

(a) (b)

Figure 6. Bending strain on the surfaces of the piezoelectric transducers for applied electric potential. Axial (a) and transverse (b) strains and corresponding linear trends are reported for measures taken in the static and quasi-static ($6Hz$) conditions.

	Applied Voltage			Applied Displacement		
	ε_1/V $(\mu\varepsilon/\,\mathrm{V}\,)$	ε_2/V $(\mu\varepsilon/\,\mathrm{V}\,)$	$\varepsilon_2/\varepsilon_1$	ε_1/V $(\mu\varepsilon/\,\mathrm{mm}\,)$	ε_2/V $(\mu\varepsilon/\,\mathrm{mm}\,)$	$\varepsilon_2/\varepsilon_1$
Exp.Static	0.72 ± 0.05	0.75 ± 0.03	1.04	57.2 ± 0.5	-18.0 ± 0.3	-0.32
Exp.Quasi-Static	0.69 ± 0.01	0.66 ± 0.01	0.96	$-$	$-$	$-$
Present Model	0.60	0.65	1.08	58.2	-18.7	-0.32
NS Model	0.61	1.36	2.23	58.2	-19.9	-0.34

Table 7. Axial and transverse strain at the surface of the piezoelectric element measured either for applied electric voltage or for applied tip displacement. Experimental values are compared to the estimates of the present model and the NS model. The confidence intervals (95 refer to the regression analysis of the data reported in Figures 6 and 7.

Applied displacement Figure 7 reports the axial and transverse strains measured when applying a tip displacement with short-circuited piezoelectric transducers. The tip displacement is applied with increments of $0.2mm$, reaching the maximum amplitude of $2mm$.

Comments and comparisons with theoretical results Table 7 resumes the experimental results for the axial and transverse strains and comnpares them with the analytical estimates given by the present model (NSR) and the standard model assuming null transverse stress (NS). The values are reported as microstrain per Volt and microstrain per millimeter. For the two loading conditions, applied voltage and applied displacement, they are extrapolated from regression analysis of the experimental data reported in Figure 6 and 7. The theoretical estimates refer to the nominal values of the constitutive and geometric parameters given in Table 3 and in Figure 5. The analysis of Table 7 leads to the following comments:

- The present model correctly predicts the ratio between transverse and axial strains for both loading conditions. The NS model gives a good estimate for the case of applied

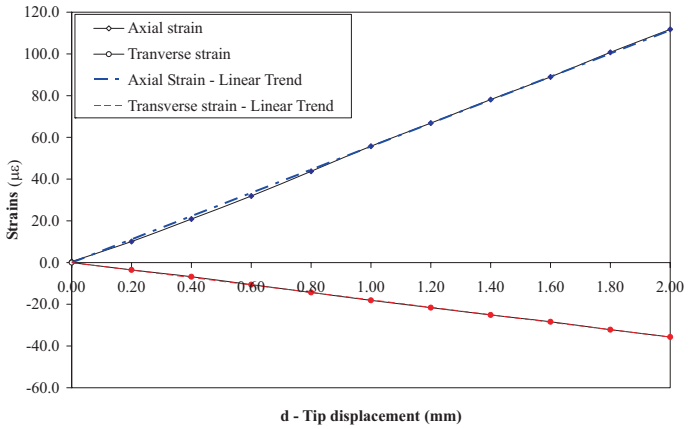

Figure 7. Axial and transverse strains for applied tip displacement under the short-circuit condition. Experimental values and corresponding linear trends are reported.

displacement, but fails in predicting the transverse strain in the case of applied potential. This is coherent to what reported, for the bimorph beam, in Figure 4 and to the qualitative sketch in Figure 2.

- The discrepancy between measured strains and theoretical estimates form the NSR model is reasonable. The theoretical analysis assumes a perfect bonding conditions and completely neglects the influence of the bonding layer. It is expected that the neglect of the bonding layer leads to a underestimate of the strain for applied displacement and an overestimate of the strain for applied voltage.
- As expected, the strain for applied voltage measured in the static case is bigger than the strain measured in the quasi-static case. This is explained by the drift phenomenon. However, the experimental data reveal an unexpected difference between the reductions of the axial and transverse strains. More accurate tests should be performed to assess if it is due to a bias in the measure of the quasi-static axial strain or if it is a real effect.

4.2 Dynamic tests: piezoelectric capacitance and resonant shunt

4.2.1 Experimental set-up

Piezoelectric elements are frequently used to damp structural vibrations. Resonant shunting is shown to be an effective mean for passive electric damping [22, 23]. Dynamic experimental tests were performed by shunting the piezoelectric element of the beam in Figure 5 on the parallel RL circuit shown in Figure 8. The beam was excited by imposing the voltage $\bar{V}(t)$ and the system response was measured by a laser vibrometer (Polytec OFV 350) targeted at the tip of the cantilever beam. The input signal was generated digitally in Labview, converted by the D/A converter National Instruments AT-MIO-16E-10, and amplified by ad-hoc designed voltage amplifier. The analog output of the laser was measured by the A/D converter National Instruments PCI-4452 and a personal computer was used for digital signal processing. To ob-

tain high-value high-quality-factor tunable inductors, an analog active RC circuit (Antoniou's circuit) was used to simulate the grounded inductive impedance of the shunting circuit (see [23] for further details).

4.2.2 Resonant shunting: 2 d.o.f.'s modal model of the beam with the shunting circuit

In a narrow frequency band around the first mechanical resonance, the beam with the piezoelectric transducer can be modelled as 1 d.o.f. system, by neglecting the influence of higher mechanical modes. Hence, the coupled electromechanical dynamics of the first mode of the beam and the shunting circuit is described by the following system of equations (see [24, 25]):

$$m\ddot{p}(t) + kp(t) - g\dot{\psi}(t) = 0 \tag{21}$$

$$C_p\ddot{\psi}(t) + \frac{1}{R}\dot{\psi}(t) + \frac{1}{L}\psi(t) + g\dot{p}(t) = \frac{1}{R}\bar{V}(t) \tag{22}$$

where $p(t)$ is the Fourier coefficient of the first bending mode of the beam, $\psi(t)$ is the flux-linkage (time primitive of the electric potential) at the electric terminal of the piezoelectric element, $\bar{V}(t)$ is the exciting voltage applied as in Figure 8, m and k are the modal mass and stiffness of the first bending mode of the beam, g is the modal piezoelectric coupling coefficient. R and L are the resistance and the inductance of the shunting circuit. The capacitance C appearing in the equation (22) is the inherent piezoelectric capacitance for blocked axial displacement. Referring to electromechanical constitutive equations (11), it is given by

$$C_p = \varepsilon_{qV} l_p \tag{23}$$

where $l_p = 36.2\,\mathrm{mm}$ is the length of the piezoelectric element. The electrical and mechanical natural frequencies coincide when the inductor is tuned to the value

$$L_{opt} = \frac{1}{\omega_1^2 C_p} \tag{24}$$

where $\omega_1^2 = k/m$ is the first mechanical resonance for the piezoelectric transducer kept at constant voltage (e.g. short-circuited). If the resistance R is sufficiently high, when $L = L_{opt}$ the modulus of the beam mobility function (tip velocity over applied voltage) has the characteristic pattern reported in Figure 8, with two picks are at the same height [22, 23]. This condition optimizes the energy transfer between the mechanical and the electric forms by an internal resonance. It is imposed to obtain efficient electric dynamic absorbers of mechanical vibrations [22]. For this reason, the knowledge of the piezoelectric capacitance C_p is important in designing passive shunt circuits.

4.2.3 Inherent piezoelectric capacitance

The inverse relation of equation (24) allows for an accurate experimental identification of the inherent piezoelectric capacitance C_p by the measures of the first mechanical resonance frequency ω_1 and of the inductance L_{opt} for which the two picks of the mobility function are at the same height. For the present experimental set-up the following values for the first beam resonance frequency and the inductance satisfying the tuning condition (24) are found:

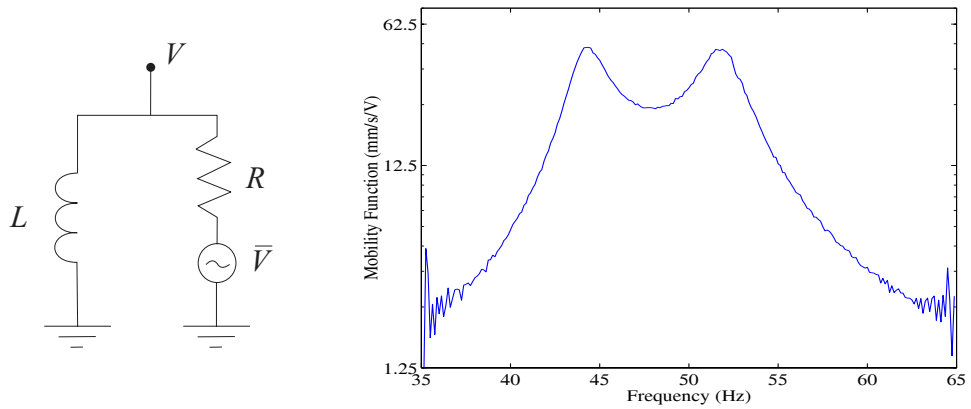

(a) (b)

Figure 8. Parallel RL shunting circuit with voltage excitation (a) and experimental frequency response (b) for the beam with the resonant circuit having $L = 103.5H$, $R = 1M\Omega$.

	Experimental	Present model	NS model
C_p	$109.4\,\mathrm{nF}$	$103.4\,\mathrm{nF}\ (-5.50\%)$	$134.0\,\mathrm{nF}\ (+22.47\%)$

Table 8. Inherent piezoelectric capacitance for the piezoelectric transducer on the beam in Figure 5. The experimentally identified capacitance is compared with the theoretical estimates.

$$f_1 = \frac{\omega_1}{2\pi} = 47.3\,\mathrm{Hz}, \quad L = 103.5\,\mathrm{H}\,.$$

The corresponding values of the piezoelectric capacitance satisfying (24) is reported in Table 8. It is compared with the theoretical estimates obtained with the proposed model accounting for the influence of transverse stress (equation (12c)) and the standard NS model assuming the uniaxial stress condition. Table 8 shows the improvement obtained with the present modelling approach.

5 CONCLUSIONS

This paper studied the influence of cross-sectional deformations in beam models of piezoelectric laminates. Numerical and experimental analyses have shown that the hypotheses on the mechanical strains and stresses which are usually accepted in the technical literature are not physically grounded. They lead to relevant errors in the estimate of the electric and mechanical constitutive properties because they do not properly account for transverse (chordwise) interactions between different layers. An Euler-Bernoulli-like beam model properly including the effect of cross-sectional deformations and of the induced electric potential was proposed. The model keeps the same degrees-of-freedom of a standard Euler-Bernoulli electromechanical theory, but introduces further hypotheses in the distribution of the electromechanical fields

through a mixed variational principle. This allows to get a closer agreement with 3D theories and experimental results. Main corrections are shown for the estimate of the equivalent piezoelectric capacitance, which is an important parameter in the design of many control systems. This is achieved by properly accounting for the effect of transverse deformations, as confirmed by numerical and experimental strain analysis.

6 ACKNOWLEDGEMENTS

The present work has been done in the framework of the joint research project "Smart materials and structures: structural control using distributed piezoelectric transducers and passive electric networks" funded by the international agreement between CNRS (France) and CNR (Italy), project #16283. Also the partial support of the MIUR (Ministero per l'Innovazione, l'Università e la Ricerca) under the PRIN project "Metodi innovativi per l'analisi e il controllo di sistemi vibroacustici" (#200309593_2004) is gratefully acknowledged.

REFERENCES

[1] E.F. Crawley, E.H. Anderson, Detailed models of piezoceramic actuation in beams, *Journal of Intelligent Material Systems and Structures,* 1, 12-25 (1990).

[2] Q.M. Wang, L.E. Cross, Constitutive equations of symmetrical triple layer piezoelectric benders, *IEEE trans. on Ultrasonics, ferroelectrics, and frequency control,* 46 (6), 1343-1351 (1999).

[3] J.G. Smits, S.I. Dalke, T.K. Cooney, The constitutive equations of piezoelectric bimorphs, *Sensors and Actuators A,* 28, 41-61 (1991)

[4] P.J. Costa Branco, J.A. Dente, On the electromechanics of a piezoelectric transducer using a bimorph cantilever undergoing asymmetric sensing and actuation, *Smart Materials and Structures,* 13, 631-642 (2004).

[5] P. Gaudenzi, R. Carbonaro, E. Benzi, Control of beam vibrations by means of piezoelectric devices: theory and experiments, *Composite Structures,* 50, 373-379 (2000).

[6] P. Lu , K.H. Lee, An alternative derivation of dynamic admittance matrix of piezoelectric cantilever bimorph. *Journal of Sound and Vibrations,* 266, 723-735 (2003).

[7] J.K. Park and W.K. Moon, Constitutive relations for piezoelectric benders under various boundary conditions. *Sensors and Actuators A,* 117, 159-167 (2005).

[8] M. Krommer, On the correction of the Bernoulli-Euler beam theory for smart piezoelectric beams. *Smart Materials and Structures,* 10, 668-680 (2001).

[9] K.Y. Sze, X.M. Yang and H. Fan, Electric assumptions for piezoelectric laminate analysis. *International Journal of Solids and Structures,* 41, 2363-2382 (2004).

[10] S. Kapuria, P.C. Dumir and A. Ahmed, An efficient coupled layerwise theory for dynamic analysis of piezoelectric composite beams, *Journal of Sound and Vibration,* 261, 927-944 (2003).

[11] Z.K. Kusculuoglu, B. Fallahi and T.J. Royston, Finite element model of a beam with a piezoceramic patch actuator, *Journal of Sound and Vibration,* 276 (1-2), 27-44 (2004).

[12] W. Beckert and G. Pfundtner, Analysis of the deformational behaviour of a bimorph configuration with piezoelectric actuation, *Smart Materials and Structures,* 11, 599-609 (2002).

[13] A. P. F.Bernhard and I. Chopra, Analysis of Bending-Torsion Coupled Actuator for a Smart Rotor with Active Blade Tips, *Smart Materials and Structures,* 10 (1), 35–52 (2001).

[14] J. Sirohi and I. Chopra, Fundamental behavior of piezoceramic sheet actuators. *J Intell Mater Syst Struct,* 11, 47–61 (2000).

[15] V. Giavotto, M. Borri, P. Mantegazza, G. Ghiringhelli, V. Carmaschi, G.C. Maffioli, and F. Mussi, Anisotropic beam theory and applications, *Computers and Structures*, 16, 403-413 (1983).

[16] L.V. Berdichevsky, *Variational principles of continuum mechanics*, Nauka, Moskow (1983).

[17] C.E.S. Cesnik and S.J. Shin, On the Modeling of Integrally Actuated Helicopter Blades, *International Journal of Solids and Structures*, 38 (10), 1765-1789 (2001).

[18] G.L. Ghiringhelli, P. Masarati and P. Mantegazza, Characterization of Anisotropic, Non-Homogeneous Beam Sections with Embedded Piezo-Electric Materials, *Journal of IntelligentMaterial Systems and Structures*, 8 (10), 842–858 (1997).

[19] C. Maurini, J. Pouget and F. dell'Isola, On a model of layered piezoelectric beams including transverse stress effect, *International Journal of Solids and Structures*, 41 (16-17), 4473-4502 (2004).

[20] C.Maurini, J.Pouget and F.dell'Isola, Extension of the Euler-Bernoulli model of piezoelectric laminates to include 3D effects via a mixed approach, accepted for publication to *Computers and Structures*.

[21] E. Reissner, On a certain mixed variational theorem and a proposed application, *International Journal for Numerical Methods in Engineering*, 20, 1366-1368 (1984).

[22] N.W. Hagood and A. von Flotow, Damping of structural vibrations with piezoelectric materials and passive electrical networks. *Journal of Sound and Vibration,* 146 (2), 243-268 (1991).

[23] F. dell'Isola, C. Maurini and M. Porfiri, Passive damping of beam vibrations through distributed electric networks and piezoelectric transducers: prototype design and experimental validation, *Smart Materials and Structures*, 13 (2), 299-308 (2004).

[24] C. Maurini, M. Porfiri and J. Pouget, Numerical and experimental methods for modal analysis of stepped piezoelectric beams, submitted to *Journal of Sound and Vibration.*

[25] C. Maurini, M. Porfiri and J. Pouget, Modal analysis of stepped piezoelectric beams with applications to electric vibration damping, *Twelfth International Congress on Sound and Vibration*, 11–14 july 2005, Lisbon (Portugal), CD-Rom, Paper N.356.